The Influence of Submeso Processes on Stable Boundary Layer Similarity Relationships

OTÁVIO C. ACEVEDO

Universidade Federal de Santa Maria, Santa Maria, Brazil

FELIPE D. COSTA

Universidade Federal do Pampa, Alegrete, Brazil

PABLO E. S. OLIVEIRA, FRANCIANO S. PUHALES, GERVÁSIO A. DEGRAZIA, AND DÉBORA R. ROBERTI

Universidade Federal de Santa Maria, Santa Maria, Brazil

ABSTRACT

Previous observational studies in the stable boundary layer diverge appreciably on the values of dimensionless ratios between turbulence-related quantities and on their stability dependence. In the present study, the hypothesis that such variability is caused by the influence of locally dependent nonturbulent processes, referred to as submeso, is tested and confirmed. This is done using six datasets collected at sites with different surface coverage. The time-scale dependence of wind components and temperature fluctuations is presented using the multiresolution decomposition, which allows the identification of the turbulence and submeso contributions to spectra and cospectra. In the submeso range, the spectra of turbulence kinetic energy range increases exponentially with time scale. The exponent decreases with the magnitude of the turbulent fluctuations at a similar manner at all sites. This fact is used to determine the smaller time scale with relevant influence of submeso processes and a ratio that quantifies the relative importance of such nonturbulent processes with respect to turbulence. Based on that, values for the local stability parameter that are unaffected by nonturbulent processes are found. It is shown that the dimensionless ratios do not usually converge to a given value as the time scale increases and that it is as a consequence of the locally dependent submeso influence. The ratios and their stability dependence are determined at the time scales with least influence of nonturbulent processes, but significant site-to-site variability persists. Combining all datasets, expressions for the dependence of the dimensionless ratios on the local stability parameter that minimize the role of the submeso contribution are proposed.

1. Introduction

In the stable boundary layer, turbulence may be restrained to quite small temporal and spatial scales. Under very stable conditions, the upper time-scale limit for turbulent processes may be as small as 5–10 s (Acevedo et al. 2007; Mahrt 2009, 2011). Nonturbulent atmospheric motions of scales larger than that, but much smaller than those traditionally classified as "mesoscale" become very important in those conditions, and have been referred to as "submeso" in recent years (Mahrt 2009; Mahrt and Mills 2009; Belušić and Güttler 2010). This is a broad definition, which encompasses processes with different physical origins that may coexist in the nocturnal boundary layer, such as gravity waves, density currents, and meandering, canopy-generated roll vortices.

Submeso processes are highly variable and site dependent, being influenced by local surface features, such as terrain and vegetation (Monti et al. 2002; Vickers and Mahrt 2007; Mahrt 2009). They may have a significant influence on the turbulence field, especially at the very stable boundary layer, when a good portion of the nocturnal turbulence may originate from the wind shear induced by nonturbulent low-frequency motion (Conangla et al. 2008; Mahrt 2010; Vindel and Yagüe 2011). In the submeso range, some important flow variables such as velocity variances or vertical fluxes do not relate in a

Corresponding author address: Otávio C. Acevedo, Departamento de Física, Universidade Federal de Santa Maria, Av Rorarima 1000, Santa Maria RS 97105-900, Brazil.
E-mail: otavio@ufsm.br

simple manner to mean-flow quantities such as vertical gradients. For this reason, the submeso contribution must ideally be removed for the quantification of stable boundary layer similarity relationships (Vickers and Mahrt 2003, 2007). The relevance of submeso motions in the stable boundary layer has historically posed difficulties to the determination of similarity relationships associated with horizontal velocity components. In that regard, Panofsky (1973) stated that "the behavior of horizontal velocity components is quite confusing," that "the low-frequency contributions to their variances do not appear to obey Monin–Obukhov scaling, so that the variances follow no clear pattern now discernible," and finally that "since the low frequencies are responsible for a large portion of the variances, the horizontal velocity variances do not obey Monin–Obukhov scaling either." Adding to that problem, the horizontal velocity variances are not the only quantities affected by submeso processes. Relevant and highly variable submeso fluxes usually exist in stable conditions, affecting, among other variables, the friction velocity u_* (Acevedo et al. 2009), which, as a scaling variable in Monin–Obukhov similarity theory, is present in most similarity expressions that relate turbulent quantities in the stable boundary layer. For this reason, all similarity relationships are subject to be influenced at a lesser or greater degree by nonturbulent processes. The local character of those processes contrasts with the universal nature that a similarity relationship must ideally possess.

Turbulence parameterizations in atmospheric boundary layer models are usually based in similarity relationships that relate high-order statistical moments to lower-order ones, or that merely compare different turbulent quantities. In 1.5-order closure models, for instance, it is usual to explicitly solve the turbulence kinetic energy (TKE) prognostic equation, and then use the predicted TKE to determine other quantities, such as u_*, through a similarity-derived value or expression for the ratio $\mathrm{TKE}u_*^{-2}$ (Wyngaard 1975; Duynkerke 1988; Andrén 1990; Cuxart et al. 2006; Baas et al. 2008; Costa et al. 2011; among others). More generally, Monin–Obukhov similarity relationships are used to parameterize the turbulent processes near the surface in all sorts of simulations of atmospheric flows, including large-eddy simulation, mesoscale, dispersion, weather forecast, and climate models. The dependence of dimensionless gradients on the Monin–Obukhov stability parameter zL^{-1}, expected to be universal, is highly variable among observational studies of the stable boundary layer. There is no observational agreement even on the neutral value ($zL^{-1} = 0$) of simple dimensionless ratios. A review made by Panofsky and Dutton (1984) found that, over flat terrain, the neutral value of ratio $\sigma_u u_*^{-1}$ varied between 2.2

and 2.5, $\sigma_v u_*^{-1}$ varied between 1.73 and 2.20, and even the ratio $\sigma_w u_*^{-1}$, not influenced by the large fluctuations of the horizontal wind components, varied between 1.20 and 1.40 among the different studies. When observations over rolling terrain are also considered, the variability is largely enhanced. Accordingly, Dias et al. (1995) reported that different previous observational studies found the neutral value of $\sigma_w u_*^{-1}$ varying between 1.14 and 1.50 and that $\sigma_\theta \theta_*^{-1}$ varied between 1.77 and 3.00.

The hypothesis to be tested at the present study is that, following the reasoning by Panofsky (1973), the observed site-to-site variability of those values and of the corresponding similarity expressions is caused by the locally dependent influence of the low-frequency, submeso processes. To test the hypothesis, turbulence data from six different locations, with variable types of surface coverage, are compared. It is important to notice that, in each case, only one observational point is used horizontally, so that the variability is only observed in the time domain. Submeso motion may be semistationary, therefore not satisfying Taylor's hypothesis, so that the temporal and spatial structures may differ appreciably, as shown by Thomas (2011). The present study, therefore, addresses only the temporal scales of the submeso flow.

The sites are described in section 2 along with the data analysis techniques. Submeso contributions to variances and covariances are evaluated in section 3, using the multiresolution decomposition, a technique that allows quantifying how events having different time scales contribute to a given statistical moment. In section 4, relevant submeso scales are defined and evaluated for each site considered. The hypothesis is finally tested in section 5, where the dimensionless ratios are shown as a function of time scale and the values that minimize the influence of submeso effects are determined and compared. Based on those findings, the data from all sites are used together to formulate alternative similarity expressions for the dimensionless ratios as a function of the stability parameter that are as unaffected by low-frequency nonturbulent processes as possible.

2. Datasets and methods

a. Measurements

Data from six different sites are compared (Table 1). Three of them (Manaus, Uatumã, and Km77) are in the Amazon region, two are in southern Brazil (Cruz Alta and São João), and one [Flux Over Snow Surfaces (FLOSS)] is in Colorado state. Surface covers are also variable. At Manaus, Uatumã, and São João the sensors

TABLE 1. Location and characteristics of the sites used in this study. For sites FLOSS and Cruz Alta, the mean nocturnal wind speed refers to the 5-m level.

	Coordinates	Surface type	Canopy height (m)	Roughness length (m)	Mean nocturnal wind speed (m s^{-1})	Reference
Cruz Alta	28°36′13″S, 53°40′25″W	Agricultural (maize)	1	0.15	2.12	Teichrieb et al. (2013)
FLOSS	40°39′32″N, 106°19′26″W	Snow	—	0.002	3.70	Mahrt and Vickers (2005)
Km77	3°72′00″S, 54°32′13″W	Pasture	—	0.03	0.52	Sakai et al. (2004)
Manaus	2°36′33″S, 60°12′33″W	Rain forest	40	2.1	1.31	Araujo et al. (2002)
São João	25°34′18″S, 50°05′56″W	Pine forest	25	—	0.85	Oliveira et al. (2013)
Uatumã	2°08′36″S, 59°00′02″W	Rain forest	35	—	0.70	—

are located above forest canopies, while the Cruz Alta dataset was collected above a maize canopy, Km77 is above a pasture, and FLOSS measurements were taken above grass that was covered by snow during part of the period. More information on the sites, including effective roughness length and mean nocturnal wind speed, is given in Table 1, where references that describe each one in further detail are also provided.

Data from seven different levels from FLOSS experiment were used, while two different levels were available at Cruz Alta. At the other four experiments, data from a single level have been considered. Although observations within the canopies were also available in some cases, these are not included in the present study. Additional details on the measurements are provided in Table 2.

b. Analysis

The data sampling rate was 60 Hz at FLOSS and 10 Hz for all other experiments. For FLOSS, the data used for the purpose of the present study went from 2000 to 0543 LST in the following morning, so that eight series of 2^{18} data points were used at each night. For the other experiments, the nocturnal period considered started at 2100 LST and ended at 0512 LST in the following morning, so that in each night there were nine series of 2^{15} data points. For these reasons, each series used from FLOSS has a time length of 1 h 13 min, while the series from the other experiments are approximately 55 min long.

Data from each series are decomposed into typical time scales using the multiresolution (MR) decomposition (Mallat 1989; Howell and Mahrt 1997). The method

and its implementation have been detailed by Vickers and Mahrt (2003). A very important property of the method is that when it is applied to a time series of length T, the integration of the MR spectra up to timescale T equals the variance of the original signal. Accordingly, integration of the MR cospectra between two variables equals the covariance between them. Moreover, the integration of the MR (co)spectra up to a timescale $\tau < T$ equals the average (co)variance of t-long subsets within the original series. In the present study, the MR decomposition is applied to time series of the three wind components u, v, w and temperature T, generating the respective MR spectra $S_u(\tau)$, $S_v(\tau)$, $S_w(\tau)$ and $S_\theta(\tau)$, each of them a function of the time-scale τ. Besides, the MR cospectra between the vertical velocity w and each of the other variables is also evaluated, being represented by $C_{uw}(\tau)$, $C_{vw}(\tau)$, and $C_{wT}(\tau)$. From these calculations, some derived quantities are determined, such as the TKE spectra $S_e(\tau) = 0.5(S_u + S_v + S_w)$ and the friction velocity (u_*) cospectra $C_{u*}(\tau) = (C_{uw}^2 + C_{vw}^2)^{1/4}$. Variables $\sigma_w(\tau)$, $\sigma_V(\tau) = [\sigma_u^2(\tau) + \sigma_v^2(\tau)]^{1/2}$, $\sigma_\theta(\tau)$, $e(\tau)$, $u_*(\tau)$, and $\overline{w'\theta'}(\tau)$ and the dimensionless ratios between them are also determined as a function of the time scale using the MR decomposition. For that purpose, each variable is obtained through the appropriate integration of the MR spectra and cospectra from τ_0, the smallest time scale available from the decomposition, which depends on the data sampling rate, to τ:

$$\sigma_i(\tau) = \left[\sum_{t=\tau_0}^{\tau} S_i(t) \right]^{1/2},$$

TABLE 2. Characteristics of the observations and data at each site.

	Sensor height(s) (m)	Sampling frequency (Hz)	Period of data	Number of series
Cruz Alta	2.5 and 5	10	December 2010–March 2011	336
FLOSS	1, 2, 5, 10, 15, 20, and 30	60	November 2002–April 2003	612
Km77	8.5	10	January–October 2001	733
Manaus	53	10	January–April 2006	185
São João	32	10	October 2009–April 2012	501
Uatumã	42	10	February–June 2012	402

$$e(\tau) = 0.5 \left[\sum_{t=\tau_0}^{\tau} S_u(t) + \sum_{t=\tau_0}^{\tau} S_v(t) + \sum_{t=\tau_0}^{\tau} S_w(t) \right],$$

$$u_*(\tau) = \left\{ \left[\sum_{t=\tau_0}^{\tau} C_{uw}(t) \right]^2 + \left[\sum_{t=\tau_0}^{\tau} C_{vw}(t) \right]^2 \right\}^{1/4},$$

$$\overline{w'\theta'}(\tau) = \sum_{t=\tau_0}^{\tau} C_{w\theta}(t), \quad \text{and}$$

$$\theta_*(\tau) = \frac{\overline{w'\theta'}(\tau)}{u_*(\tau)},$$

where $i = u, v, w,$ or θ.

At this point, it is important to notice that the term TKE (and the corresponding symbol e) is used to refer to half of the sum of the variances of the wind component perturbations, following common practice in micrometeorological literature. However, as both turbulent and nonturbulent modes may contribute to the horizontal variances, the variable referred here as TKE is not purely turbulent.

Throughout most of the paper, the variables are classified in terms of the standard deviation of the vertical velocity component σ_w, chosen because it is least affected by the submeso processes being compared (Acevedo et al. 2009). For such a classification, σ_w is obtained from the integration of $S_w(\tau)$ over all time scales considered. Other stability indicators, such as the flux Richardson number or the Obukhov length, would be largely affected by the low-frequency variability, especially at the larger limit of time scales considered in the present study. The gradient Richardson number would be a more viable option, but it is not available at the four sites where only one observation level exists. Nevertheless, it is important to use a stability index to compare the present results with previous ones, and for that purpose the local stability parameter $z\Lambda^{-1}$ is used, where $\Lambda \equiv -\overline{\theta} u_*^3 / (\kappa g \overline{w'\theta'})$ is the local Obukhov length, determined from the local values of friction velocity u_* and heat flux $\overline{w'\theta'}$. It is carefully determined for each class of σ_w from its time-scale dependence, using a method detailed and shown to be robust in section 4.

When a comparison between the sites is performed, 10 values are used from each site, corresponding to 10 classes of σ_w, each of them containing $^1/_{10}$ of the total time series. The reason for doing that is to avoid over-representing datasets with more time series available. Therefore, when such comparisons are made, each point represents the average over a large number of time series of similar σ_w—a procedure that has been employed

by Mahrt et al. (2013) using the gradient Richardson number as the classifier index.

3. Average spectra

Of all sites, the least turbulent is Km77, located at a deforested area in Amazonia where the large radiative loss creates a very stable boundary layer at night (Sakai et al. 2004; Acevedo et al. 2007). At this site, the mean σ_w is only $0.092 \pm 0.016 \, \mathrm{m \, s^{-1}}$. The three forested sites have approximately the same average σ_w: $0.20 \pm 0.036 \, \mathrm{m \, s^{-1}}$ at Uatumã, $0.22 \pm 0.042 \, \mathrm{m \, s^{-1}}$ at Manaus, and $0.23 \pm 0.055 \, \mathrm{m \, s^{-1}}$ at São João. The two most turbulent sites are Cruz Alta, where the mean σ_w is $0.28 \pm 0.071 \, \mathrm{m \, s^{-1}}$ at the 2.5-m level and $0.27 \pm 0.062 \, \mathrm{m \, s^{-1}}$ at 5 m and FLOSS where mean σ_w is $0.29 \pm 0.090 \, \mathrm{m \, s^{-1}}$ at 1 m, increasing progressively with height until $0.39 \pm 0.16 \, \mathrm{m \, s^{-1}}$ at 30 m. The average TKE spectrum from each site characterizes them in terms of the role of low-frequency processes (Fig. 1). It is interesting that at FLOSS and Cruz Alta the lower-level mean σ_w, which represents the turbulent field, are very close to each other. However, at time scales larger than 100 s the TKE spectrum is always one order of magnitude larger at FLOSS than it is at Cruz Alta. Besides having larger magnitude, the intense low-frequency processes occur at smaller time scales in FLOSS than in Cruz Alta, so that, between these two sites, only in Cruz Alta a cospectral peak is visible in the average TKE spectra. Among the other sites, Km77 is the one where low-frequency TKE is closer in magnitude to FLOSS, and this may be surprising considering that these two are the least (Km77) and most (FLOSS) turbulent of all sites considered at the present study. At the other three sites, the forested ones, low-frequency processes play an intermediate role so that a cospectral gap can be defined from the average TKE spectra in all of them, but not as well as it is defined at Cruz Alta. It is not entirely clear what causes such a large variability on the influence of nonturbulent low-frequency processes at each site. At Km77, the very intense stability largely reduces the temporal and spatial scales of the turbulent flow, allowing the low-frequency processes to dominate at reasonably small scales and to usually reach appreciable intensities. Besides, being located at a pasture surrounded by forest at a few kilometers of distance, it is possible that the vegetation gradients contribute to the generation of the intense low-frequency motion observed at that site. At FLOSS, the most turbulent of the sites studied here, the same feature cannot be attributed to the stability, and Vickers and Mahrt (2007) suggested that it may be topographically generated. It is not clear why the nonturbulent low-frequency motion is so weak at the Cruz Alta site and

FLOSS

Cruz Alta, agricultural site, southern Brazil

Uatumã, 35–m Amazonian rain forest

Km 77, clearing in Amazonia region

São João, 25–m Pine forest, southern Brazil
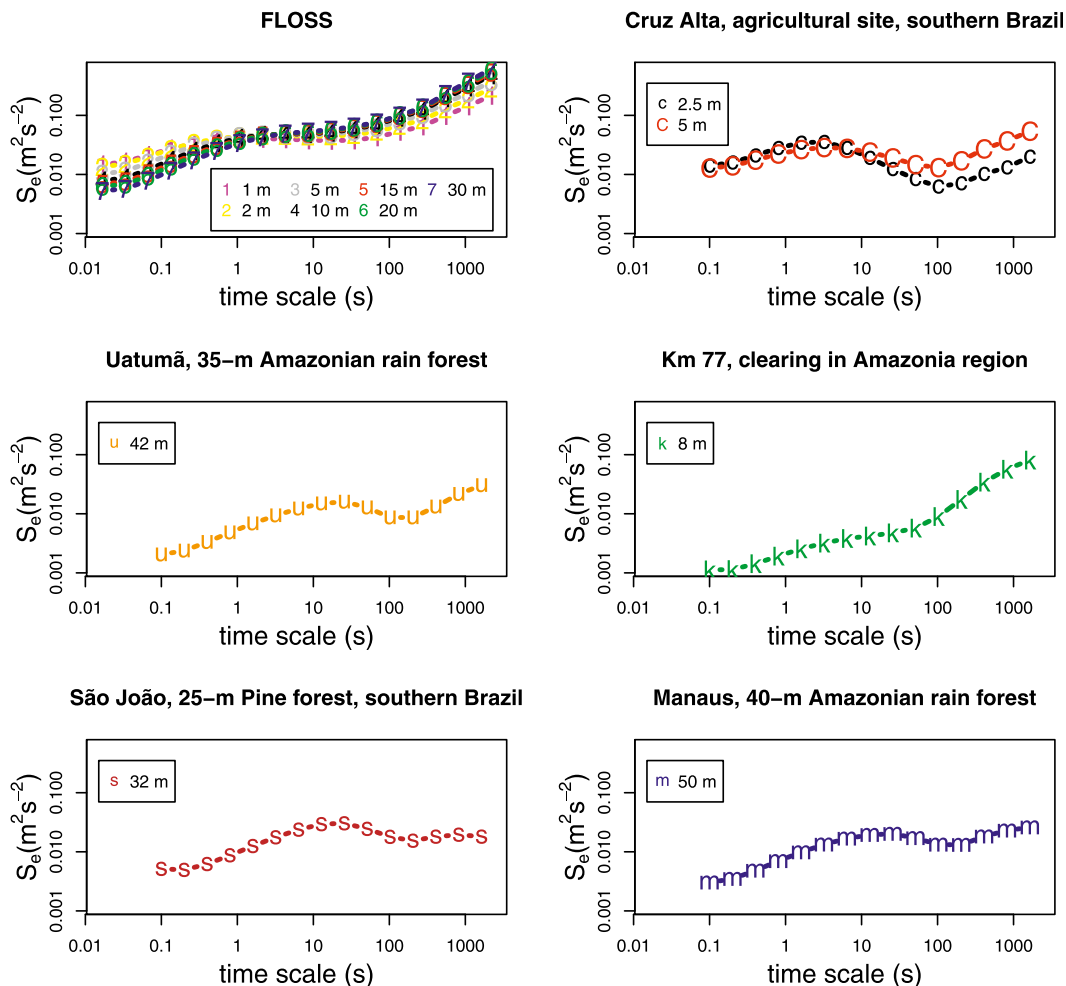
Manaus, 40–m Amazonian rain forest

FIG. 1. Average TKE spectra for each site and each level, according to legend.

a deeper analysis is certainly necessary to clarify this issue. At the three forested sites, low-frequency flow may be associated with the underlying forest, which is something that Vickers and Mahrt (2007) observed to occur at the forested sites they analyzed. In that regard, Finnigan (2010) described regular marching waves above vegetated canopies induced by the plant motion and that are very likely to be a manifestation of submeso flow. Furthermore, Finnigan et al. (2009) suggested that canopies may induce flow instabilities that generate roll-like motions, which may also be classified as submeso flow and ultimately generate turbulence. It is important to say that although Manaus and Uatumã are located above primary Amazon forest, São João site is at a small 32-ha forest sample surrounded by nonforested areas, so that the vegetation contrast may have a contribution to the low-frequency flow there. Figure 1 shows that in all sites there is a range of temporal scales in the low-frequency range where TKE increases monotonically

with time scale. From this point on, we will refer to that range as submeso, although only in section 3 a precise definition of a submeso time scale will be presented.

The average multiresolution spectra for different classes of σ_w are shown for a site with significant submeso influence (FLOSS; Fig. 2a) and for the site where such effects are least relevant (Cruz Alta; Fig. 2b). In both sites, submeso processes have little or no contribution to vertical velocity spectra (Fig. 2, top-left panels), confirming the horizontal character of submeso flow, reported by Mahrt (2010) and supporting the choice of σ_w as the variable that most purely characterizes the turbulent flow, being unaffected by larger-scale processes (Acevedo et al. 2009; Thomas et al. 2013).

Contrasting with that behavior, TKE spectra show a sudden increase with time scale at the submeso range. In FLOSS (Fig. 2a, top-right panel), for the least turbulent class, such an increase is evident at time scales as small as 10 s—well within the range of the usual
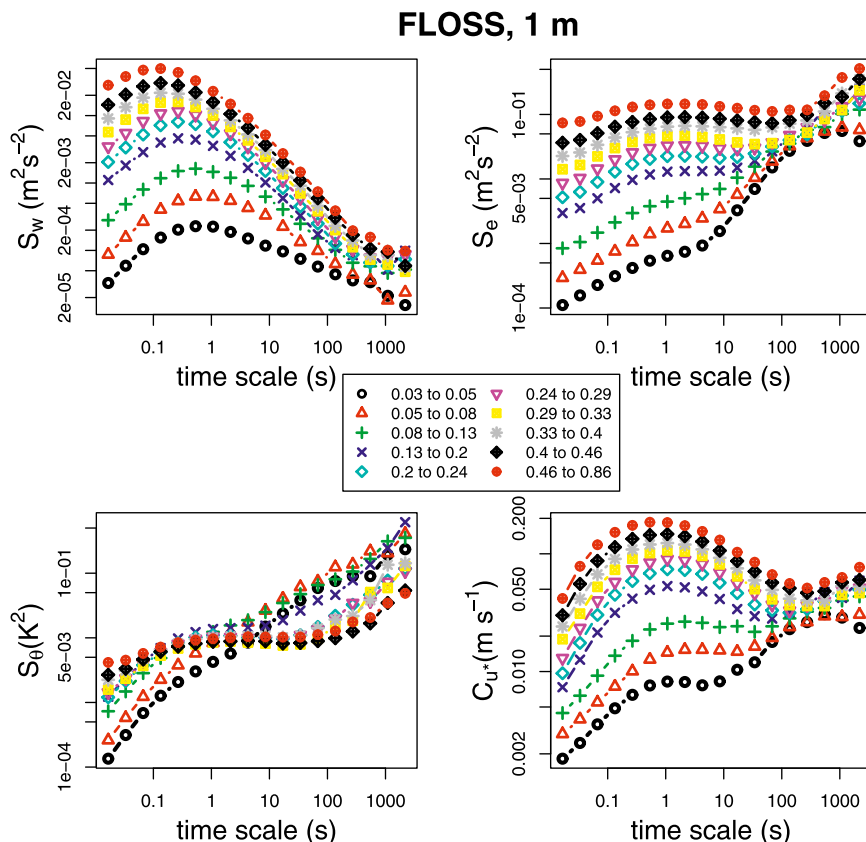
FIG. 2. (a) Multiresolution spectra of (top left) vertical velocity, (top right) TKE, (bottom left) temperature, and (bottom right) cospectra of friction velocity for the 1-m level of FLOSS project. Each line represents a different class of σ_w (m s^{-1}) as given by legend. (b) As in (a), but for 2.5-m level of Cruz Alta project.

turbulent processes. The time scale at which submeso processes become relevant increases for more turbulent conditions, reaching values larger than 100 s for the most turbulent class, but it always partially overlaps the turbulence range in a way that the TKE spectral peak cannot be easily determined for any of the 10 classes of σ_w considered. In Cruz Alta, the general characteristics of the TKE spectra and of its dependence on σ_w are similar to those observed in FLOSS, and the most relevant difference is the time scale at which the submeso processes become important—larger at Cruz Alta than in FLOSS. Such a larger time scale in Cruz Alta reflects the fact that a cospectral gap is more easily identified in this site, as the submeso processes occur at time scales larger than the TKE spectral peak for all classes. It is particularly important to notice that despite these important differences, once the submeso processes become relevant, they increase with time scale at Cruz Alta in a manner similar to that observed in FLOSS.

The temperature spectra at both sites (Figs. 2a and 2b, bottom-left panels) behave in a manner correspondent

to the TKE spectra. It means that a large S_θ increase with time scale marks the submeso range at both sites and that in FLOSS such an increase starts at smaller time scales than in Cruz Alta, with the consequence that a cospectral gap and a peak in the turbulent portion of the spectra is visible at Cruz Alta but not in FLOSS. It is important, however, to notice that in both sites the submeso increase in S_θ starts at smaller time scales than the corresponding S_e increase. This result is consistent with the finding by Thomas (2011) that temperature temporal scales are smaller than those associated to the wind field. He also found even more contrasting differences between the temperature (smaller) and wind (larger) spatial scales, and this fact suggests that submeso influence may differ even more between the temperature and wind fields spatially than they differ temporally.

The quantity C_{u*} shows the contribution of each time scale for the friction velocity. It is particularly important in the context of the present study, because u_* is the typically used velocity scale in the atmospheric surface

Cruz Alta, 2.5 m

Legend:
- 0.03 to 0.09 (○)
- 0.09 to 0.12 (△)
- 0.12 to 0.16 (+)
- 0.16 to 0.2 (×)
- 0.2 to 0.25 (◇)
- 0.25 to 0.28 (▽)
- 0.28 to 0.32 (■)
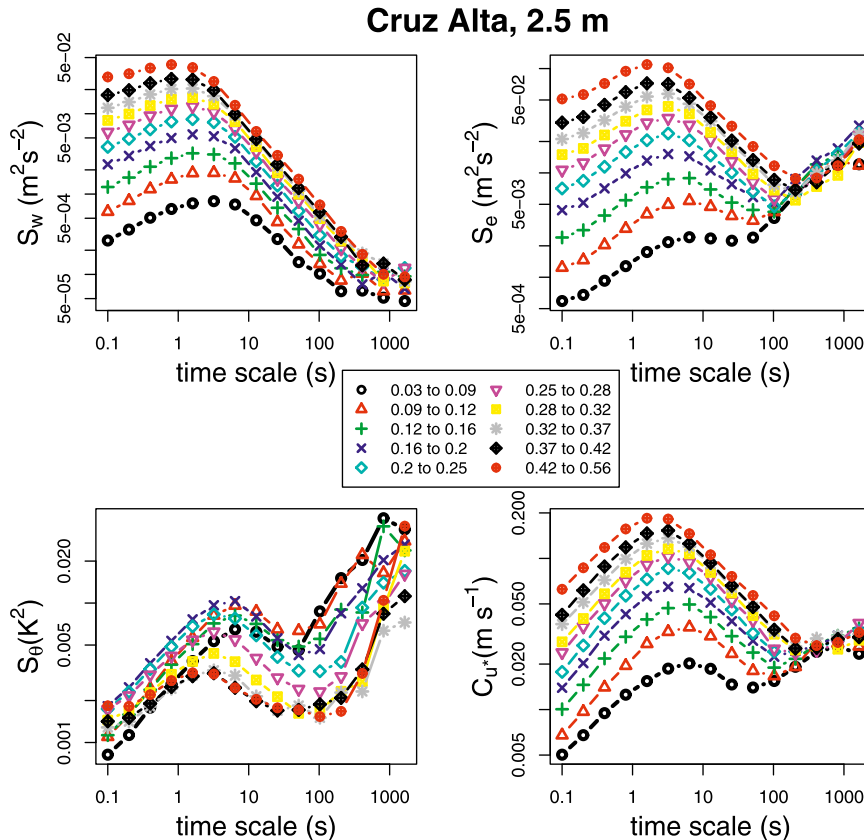- 0.32 to 0.37 (✳)
- 0.37 to 0.42 (◆)
- 0.42 to 0.56 (●)

FIG. 2. (*Continued*)

layer, so that it appears in virtually all Monin–Obukhov similarity relationships. Ideally, the quantity chosen for that purpose should not be affected by nonturbulent processes. However, as shown by Acevedo et al. (2009), u_* is, indeed, influenced by submeso processes—a consequence of the fact that the submeso momentum fluxes are usually not negligible. In both FLOSS (Fig. 2a, bottom-right panel) and Cruz Alta (Fig. 2b, bottom-right panel), C_{u*} is relevant in the submeso range, but some interesting aspects are also evident. First, the C_{u*} cospectral peak can be defined even at FLOSS—something that does not occur for the TKE cospectra as a consequence of the overlap between submeso processes and turbulence (Fig. 2a, top-right panel). Furthermore, submeso C_{u*} does not increase with time scale as much as submeso TKE does. These aspects indicate that, although submeso processes affect the friction velocity, they do so in a lesser manner than they affect TKE, indicating that vertical momentum fluxes are not as affected by submeso processes as the horizontal velocity variances are. It also suggests that the submeso flow is in many cases two dimensional, being largely dominated by the horizontal flow. Such an idea needs to be exploited in further detail in future studies,

preferably using a dataset that permits identifying the spatial structure of the flow.

Mahrt (2009) did not find a constant spectral slope for the horizontal kinetic energy in the submeso range of time scales. The same can be stated for the datasets being studied here, but a careful analysis of the rate of submeso TKE increase with time scale provides some interesting results. The TKE spectra presented in Figs. 2a and 2b (top-right panels) suggest that a power-law relationship such as $e_{sm} \propto t^k$—where e_{sm} is the TKE at the submeso range, t is the time scale, and k is a constant—is valid for a broad range of time scales. In the least turbulent class from FLOSS, for instance, it holds from time scales of 10 to more than 100 s (Fig. 3, inlet, black dots), while for the least turbulent class from Cruz Alta, where submeso processes occur at larger scales, the same can be said from 50 to 800 s (Fig. 3, inset, blue dots). In more turbulent conditions, the entire submeso interval shifts toward larger scales, but evidence from Figs. 2a,b, and from the other sites whose spectra are not shown here, indicate that the sharp TKE increase with time scale may follow the same power-law type of relationship with time scale, although in that case the exponent k may be different.
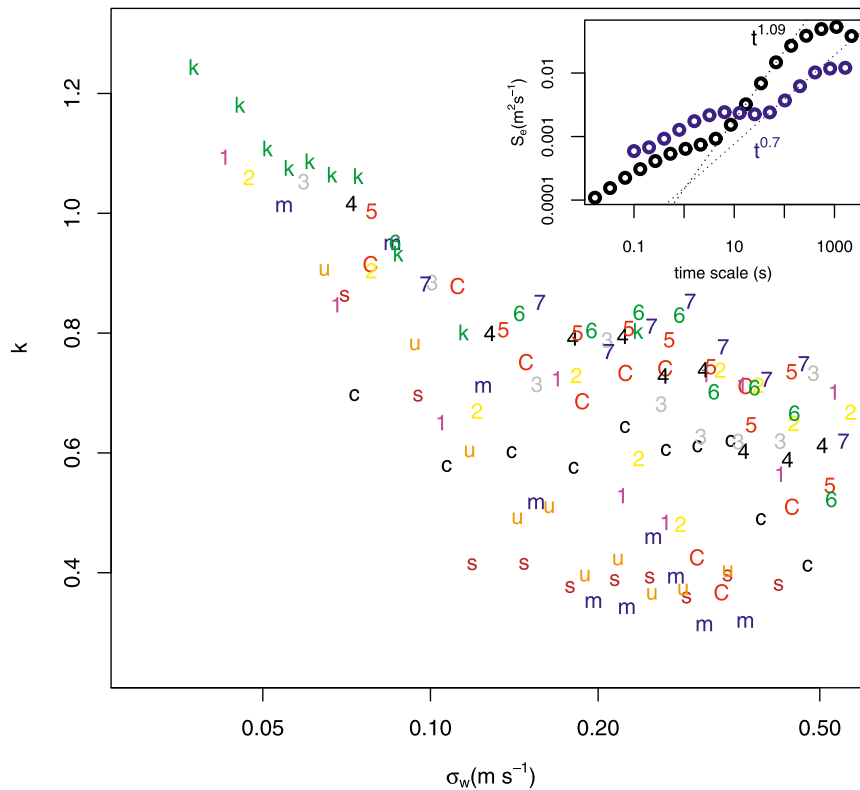
FIG. 3. Dependence of the submeso TKE spectra exponent k (see text) on σ_w. For each site and level, the points represent 10 classes of σ_w. The symbols that represent each site are the same used in Fig. 1. Inset at upper-right corner shows the TKE spectra for the least turbulent classes of FLOSS at 1 m (black dots) and of Cruz Alta at 2.5 m (blue dots); dashed lines show the submeso exponential increase.

To quantify that, the exponent k has been determined for all classes of σ_w at all sites and levels considered in the present study. It was achieved by linearly adjusting $\log(e)$ to $\log(t)$ for every four subsequent values of TKE spectra at ranges larger than 5 s and finding, in each case, which range of time scales provided the best linear fit. As an example, the slopes found for the two cases shown in the inlet of Fig. 3 are represented by dotted lines. In both of these cases, the best fit found has R^2 above 0.99. Similarly good adjustments could be obtained in the vast majority of S_e spectra analyzed, indicating the existence of a submeso range power law. In general, the exponents were highly variable, ranging from 0.4 to 1.2. Interestingly, however, they are highly dependent on σ_w, with the largest exponents happening at the least turbulent cases (Fig. 3, main panel). Furthermore, the exponents found at the different sites follow the same general dependence on σ_w. This is particularly true for the least turbulent classes of data, so that for $\sigma_w < 0.1\,\mathrm{m\,s^{-1}}$ all points from different sites and vertical levels seem to collapse in the same general functional dependence of k in terms of magnitude of the turbulent

fluctuations. For more turbulent conditions, the exponent still decreases with σ_w, but the scatter among the different sites becomes larger. In such turbulent conditions, there is a general tendency of separation between nonforested sites FLOSS (symbols 1–7) and Km77 (symbol k), with larger exponents and forested sites Manaus (m), Uatumã (u), and São João (s), where the exponents tend to be smaller. Agricultural site Cruz Alta (c and C) is more variable, ranging between the two general classes.

These results allow concluding that the TKE increase with time scale in the submeso interval is consistently larger when the stable boundary layer (SBL) is less turbulent. Such a relationship may be explained if one considers that the mesoscale (rather than submeso) flow depends on features external to the SBL, being relatively independent from the turbulent fields. In that case, at a low turbulent condition a larger submeso slope would merely be showing that in such case TKE needs to increase faster to reach an independent value toward the mesoscale range, and the opposite would occur in more turbulent situations. This is, however, a simple descriptive
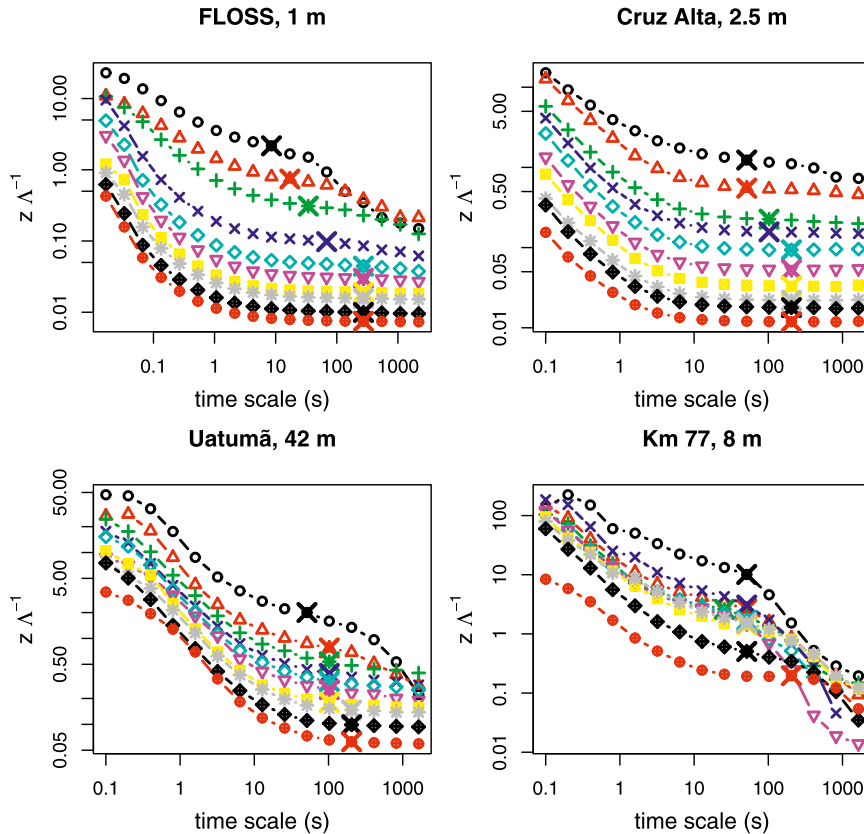
FIG. 4. Time-scale dependence of the local stability parameter $z\Lambda^{-1}$ for four different sites as shown above each panel. Each line represents a different class of σ_w (m s^{-1}), as given by legend in Fig. 2a for FLOSS and in Fig. 2b for Cruz Alta. The legend values for Uatumã and Km77 are omitted, but follow the same order as in FLOSS and Cruz Alta. The time scale t_{sm}, chosen as indicator of the beginning of the submeso range (see text), is marked at each line by a large cross.

and highly speculative explanation. More detailed analysis is necessary to conclusively explain the result.

4. Submeso time scale and relative intensity

In classical Monin–Obukhov similarity theory, atmospheric stability is quantified by the stability parameter zL^{-1}, or $z\Lambda^{-1}$ in the case of local similarity theory. In recent years, it has been identified that many of such existent similarity expressions are contaminated by self-correlation (Klipp and Mahrt 2004; Baas et al. 2006), in the sense that the dimensionless ratios analyzed are dependent of the same turbulent quantities used to define L or Λ. For that reason, more recent studies favor the use of the gradient or bulk Richardson number as a stability parameter that is independent of higher-order turbulent statistical moments (Mauritsen and Svensson 2007; Burns et al. 2010; Mahrt et al. 2013). Despite such an important, acknowledged aspect, to properly compare the present findings with other studies and with most of the similarity expressions found in literature, it is

necessary that in this study atmospheric stability is expressed in terms of the local stability parameter $z\Lambda^{-1}$. However, another difficulty arises, and it is the fact that quantities on which the local Obukhov length Λ depends, such as the local friction velocity u_* or the heat flux $\overline{w'\theta'}$, are highly influenced by nonturbulent processes in the low-frequency range. One first step to minimize this dependence was the choice of first averaging each of these variables by σ_w class and then determining the average Λ of each class—a procedure similar to what was done by Mahrt et al. (2013). This was particularly important to minimize submeso influences on the heat flux, as they can be quite large and of either sign (Vickers and Mahrt 2003), so that the averaging procedure greatly reduces its intensity in the submeso range. However, this process alone does not entirely remove the submeso influence on $z\Lambda^{-1}$. For many of the σ_w classes, especially the most turbulent ones, and in most sites, the stability parameter $z\Lambda^{-1}$ converges to a nearly constant value as the time scale increases (Fig. 4). In the most stable classes of all sites, however, the value
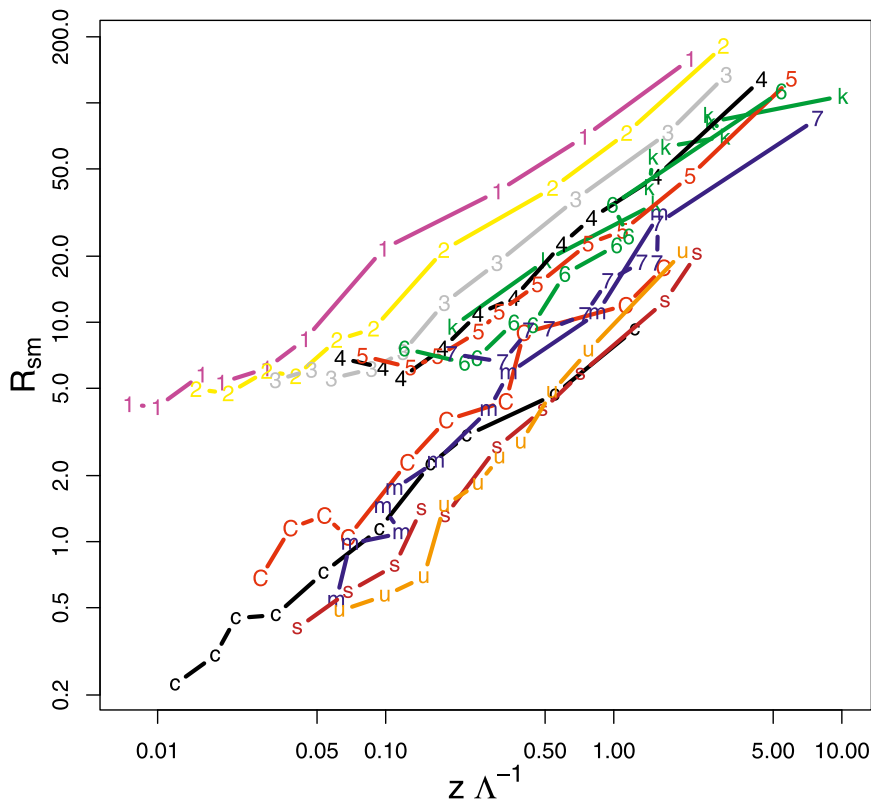
FIG. 5. Ratio R_{sm} that quantifies the relative importance of the submeso processes with respect to turbulence (see text) as a function of $z\Lambda^{-1}$ for the different sites and levels, as given by symbols described in Fig. 1. For each site and level, 10 points are plotted, corresponding to the 10 classes of σ_w considered.

of $z\Lambda^{-1}$ converges at an intermediate time scale, but suddenly decreases at the submeso range. Such a decrease occurs at the most stable classes of all sites shown in Fig. 4 at a lesser (Cruz Alta) or greater degree (FLOSS and Km77). At the very stable site of Km77 the problem is enhanced, such that there is no $z\Lambda^{-1}$ convergence at the large limit of time scale even for the most turbulent σ_w class. This means that if no effort is taken to remove the submeso influence, the stability parameter may be not representative of the true conditions of the turbulent field, and may be highly dependent on the time scale chosen for the averaging.

It is clear, therefore, that the largest time scale for which the submeso processes are not dominant with respect to the turbulent ones must be determined to properly characterize the stability parameter $z\Lambda^{-1}$, and that value will be useful to determine other quantities as well. Such a time scale will be referred as t_{sm}. In Figs. 2 and 3, it has been shown that the submeso range is characterized by a sharp TKE increase with time scale. Based on that, it is possible to find t_{sm} as the time scale when such an increase starts to happen, or the smallest of the four subsequent time scales that lead to the determination of the

power-law exponent shown in Fig. 3. In Fig. 4, it is clear that such method always finds a t_{sm} (marked by an x in each line) that is not affected by the submeso influence that is responsible by the sudden drop of $z\Lambda^{-1}$ in the larger time-scale limit. Therefore, all values of $z\Lambda^{-1}$ used in the present study are determined at time-scale t_{sm} and such choice almost completely removes the influence of submeso processes on the $z\Lambda^{-1}$ value.

It is also important to quantify the relative importance of the submeso processes with respect to the turbulent ones. With this purpose, a ratio between submeso and turbulence is defined as $R_{sm} = e_{sm}/\sigma_w^2$, where e_{sm} is the mean TKE multiresolution spectrum from t_{sm} to the largest time scale considered. In all sites, R_{sm} increases with stability, showing that submeso processes become more relevant in the very stable boundary layer (Fig. 5). Besides such stability dependency, it is also possible to identify from Fig. 5 a strong site variability regarding the relative significance of the submeso processes. Two main classes can be distinguished. Observations taken above vegetated canopies (forests São João, Manaus, and Uatumã, plus agricultural Cruz Alta) show R_{sm} relatively smaller than in the frost surface of FLOSS or the pasture
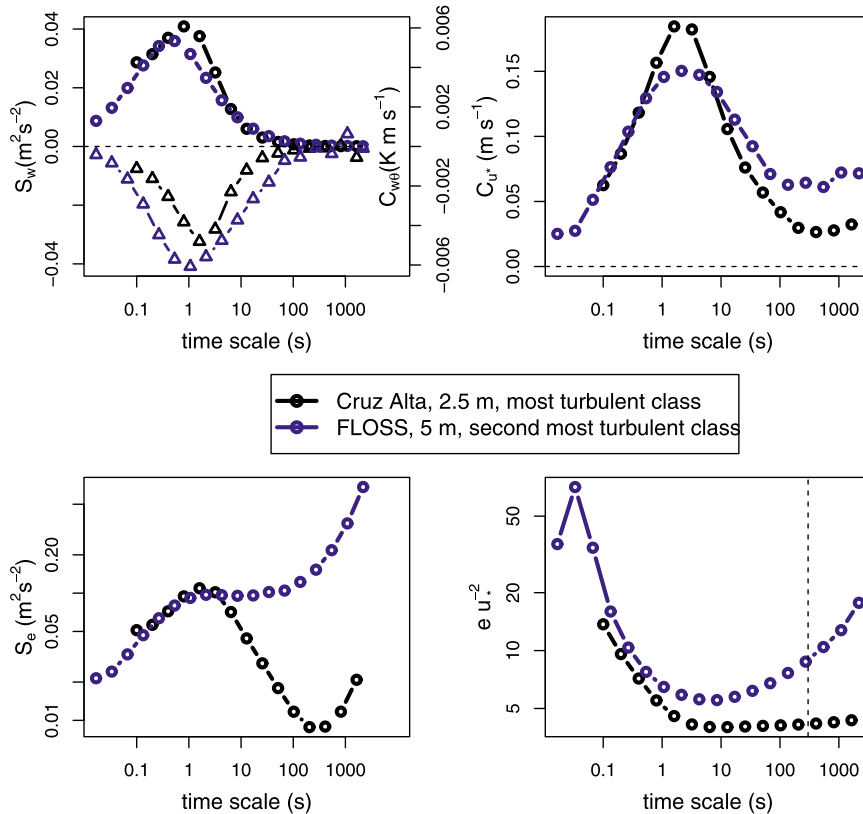
FIG. 6. Comparison between two different σ_w classes of data, one from Cruz Alta (black) and the other from FLOSS (blue), as described in legend. Variables compared are (top left) vertical velocity spectra (circles) and heat flux cospectra (triangles, axis at the right side) and (top right) friction velocity cospectra; (bottom left) TKE spectra and (bottom right) the eu_*^{-2} ratio.

of Km77. This result may partially reflect the fact that it tends to be more turbulent above canopies, but the R_{sm} difference at the neutral limit between FLOSS ($R_{sm} \approx 5$) and Cruz Alta ($R_{sm} \approx 0.2$) is much larger than the difference in σ_w between the two sites. There is, therefore, large genuine site-to-site variability of the submeso relative importance, and the results from Fig. 5 indicate that the type of surface may play an important role in that regard, which is in agreement with results from Vickers and Mahrt (2007). It is also interesting to notice that the seven levels from FLOSS (symbols 1–7 from the lowest to highest level) show an important height dependence of R_{sm}. In general, submeso processes are relatively more important with respect to turbulence at lower than higher levels, and they tend to become more constant with height as one moves up in the SBL.

5. Dimensionless ratios

a. Case studies

To illustrate how much the influence of submeso processes may affect the dimensionless ratios typically

used to characterize the turbulent field in the atmospheric boundary layer, two cases are compared. They have been chosen from the sites with most (FLOSS) and least (Cruz Alta) submeso influence among all considered here. The σ_w classes picked for the comparison from each site are such that relevant turbulent variables, such as σ_w itself and the heat flux $\overline{w'\theta'}$ are rather similar between them (Fig. 6, top-left panel). At the turbulent range, the friction velocity u_* is slightly larger for the Cruz Alta case than at the FLOSS case (Fig. 6, top-right panel). The opposite, however, occurs at time scales larger than 10 s, which is a consequence of the submeso processes—much more significant in FLOSS than in Cruz Alta. The submeso influence is most clearly perceived at the TKE spectra (Fig. 6, bottom-left panel). In that case, the spectra for both sites are almost equal up to scales near 1 s, when a drastic differentiation occurs. At FLOSS, submeso motions mask the turbulent peak of the TKE spectra, while at Cruz Alta their much more reduced magnitude allow a clear definition of the TKE spectral peak and of a spectral gap. The distinction of this variable between the two sites is such that at time
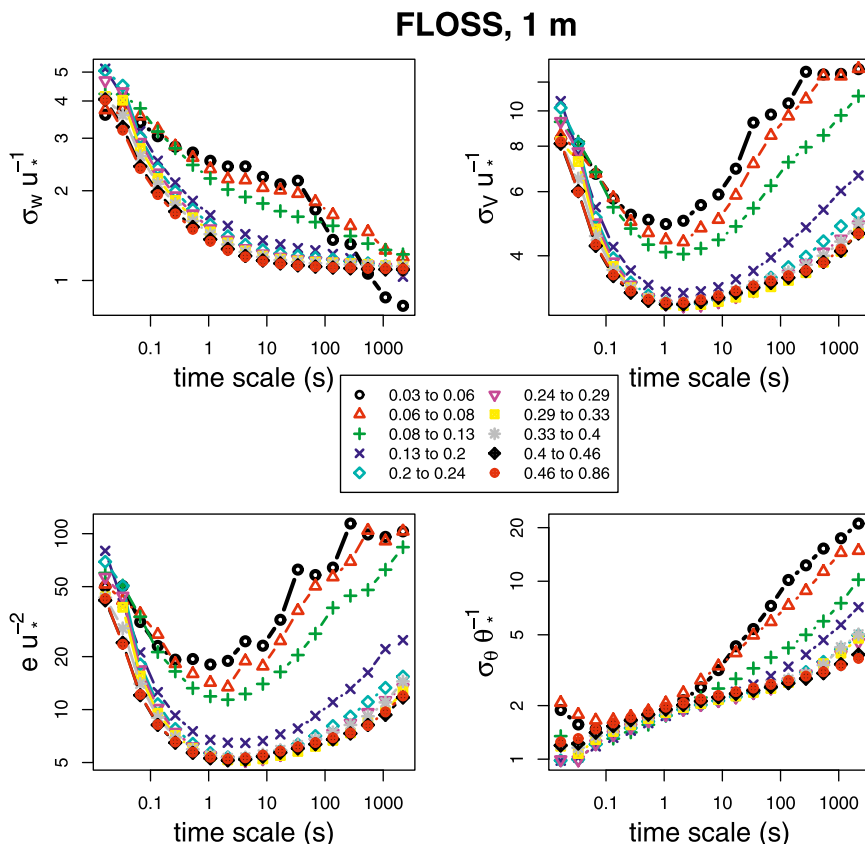
FIG. 7. (a) Ratios (top left) $\sigma_w u_*^{-1}$, (top right) $\sigma_V u_*^{-1}$, (bottom left) eu_*^{-2}, and (bottom right) $\sigma_\theta \theta_*^{-1}$ for the 1-m level of FLOSS project. Each line represents a different class of σ_w (m s^{-1}) as given by legend. (b) As in (a), but for 2.5-m level of Cruz Alta project.

scales of 100 s or larger TKE at FLOSS exceeds that of Cruz Alta by more than an order of magnitude.

It is clear, therefore, that submeso processes affect TKE much more than u_* and, for this reason, the ratio eu_*^{-2} does not converge to a constant value as the time scale increases (Fig. 6, bottom-right panel). The consequence is that the two cases being contrasted here with similar turbulence intensities and heat fluxes have rather different values of the ratio, no matter how the averaging procedure is performed. For instance, if a constant averaging time of 5 min is employed, as is usual in SBL studies of turbulence (Mahrt et al. 1998; Sun et al. 2012), the ratio eu_*^{-2} is 4.2 at the Cruz Alta case analyzed here, more than doubling at the FLOSS case, where it reaches 10.7. It is worthwhile noticing that in the FLOSS case, where submeso TKE plays a dominant role, the ratio eu_*^{-2} has a distinct minimum at intermediate time scales. This is a consequence of covariances between wind components decreasing both at very small time scales and at the submeso range much more than the correspondent variances do. In other words, at very small eddies there are fluctuations of the wind components,

but not much eddy fluxes at the same scales. Interestingly, the same holds at the submeso range, and the consequence is the minimum of the ratio eu_*^{-2} at intermediate time scales. For this reason, one may conclude that such a minimum is the value of the ratio eu_*^{-2} that best represents the turbulent field alone. It does not mean, however, that such value is totally unaffected by submeso processes, as it is clear in the FLOSS case depicted in Fig. 6 that there is significant overlap of turbulence and submeso processes for an entire interval of time scales, which encompasses the referred minimum. Nevertheless, this minimum is certainly the best possible estimate to the value of the ratio due to turbulent processes alone.

The behavior of other relevant ratios and their variability with σ_w is shown in Figs. 7a,b for the lowest vertical level of FLOSS and Cruz Alta, respectively. In the most turbulent cases, the ratio $\sigma_w u_*^{-1}$ converges in both sites to a constant value with time scale (Figs. 7a,b, top-left panels). For the least turbulent conditions, on the other hand, $\sigma_w u_*^{-1}$ decreases with time scale at the submeso range. This happens because although σ_w
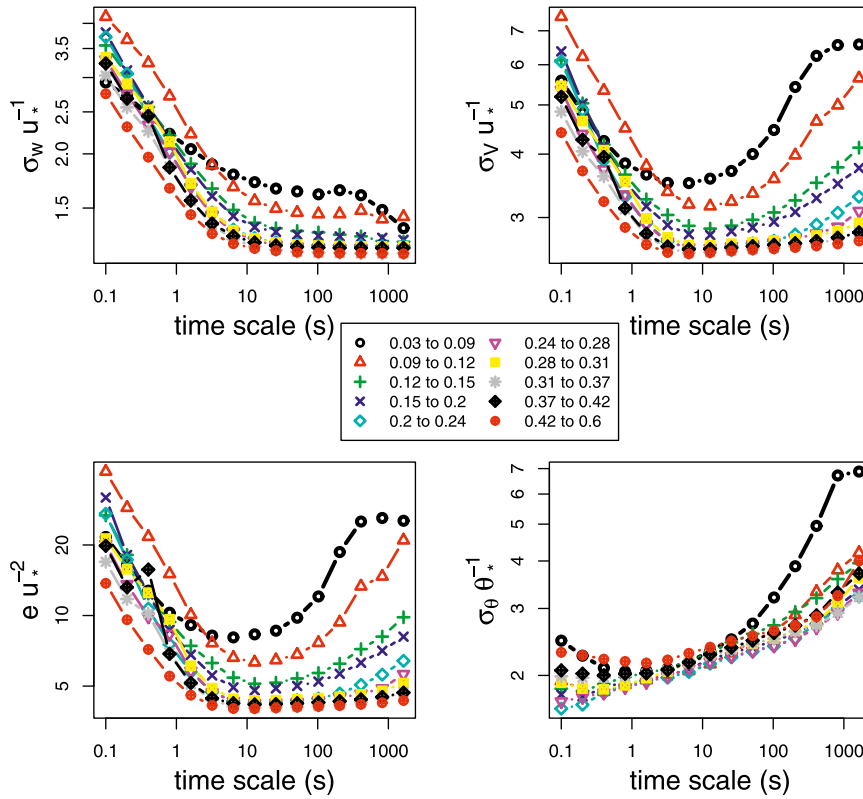
Cruz Alta, 2.5 m

FIG. 7. (*Continued*)

usually has no submeso component (as has been seen in Figs. 2a,b) and, therefore, converges to a constant value at large enough time scales, the same cannot be stated about u_*, whose submeso contribution leads to a decrease of the ratio at large time scales in the least turbulent conditions. For the horizontal wind components, on the other hand, the ratio $\sigma_V u_*^{-1}$ increases with time scale at the submeso range for all classes in FLOSS (Fig. 7a, top-right panel) and for the least turbulent ones in Cruz Alta (Fig. 7b, top-right panel). The reason is the same that explains the behavior of eu_*^{-2} in Fig. 6: submeso motion affects horizontal variances more than momentum fluxes. The dominance of horizontal submeso processes over the vertical ones causes the ratio eu_*^{-2} to behave similarly to its horizontal components, with a minimum at intermediate time scales (already seen in Fig. 6). The time scale of such a minimum is larger in more turbulent conditions, which is a consequence of lesser submeso influence and larger turbulent eddies. In all classes shown in Figs. 7a,b, the ratio $\sigma_\theta \theta_*^{-1}$ increases monotonically with time scale for time scales larger than 1 s. It is caused by the significant contribution of submeso processes to both σ_θ and u_*, seen in Figs. 2a,b, at the same time that most submeso contributions to

$\overline{w'\theta'}$ average out for a given σ_w class. The submeso influence enhances the variability of $\sigma_\theta \theta_*^{-1}$ with σ_w. In fact, both at FLOSS and Cruz Alta, there is a range of time scales (near 1 s at FLOSS, from 1 to near 100 s at Cruz Alta) for which all $\sigma_\theta \theta_*^{-1}$ curves seem to converge, suggesting that the ratio may be very weakly dependent on σ_w. This dependence will be analyzed in detail at the next subsection. It is important here to mention that the almost monotonic behavior shown for $\sigma_\theta \theta_*^{-1}$ in terms of time scale shown in Figs. 7a,b is not observed at higher levels of FLOSS and in other sites where the observation are not as close to the surface as those shown in Fig. 7. In those cases, the ratio decreases with time scale for the smallest time scales, and a $\sigma_\theta \theta_*^{-1}$ minimum is found at intermediate time scales, as happens for $\sigma_V u_*^{-1}$ and eu_*^{-2} (figures not shown).

b. Site comparison

In this subsection, the ratios discussed above are analyzed in terms of their dependence on the local stability parameter $z\Lambda^{-1}$ for the six sites considered. The main purpose of the analysis is to test the basic hypothesis of the study, that most of the site-to-site variability of such ratios may be attributed to the contribution of submeso

TABLE 3. Values of t_{sm} (s) found for each site, level, and class of σ_w, from least turbulent (C1) to most turbulent (C10) class.

	C1	C2	C3	C4	C5	C6	C7	C8	C9	C10
FLOSS, 1 m	8.5	17	34	68	273	273	273	273	273	273
FLOSS, 2 m	8.5	17	34	68	273	273	273	273	273	273
FLOSS, 5 m	17	17	34	68	68	273	273	273	273	273
FLOSS, 10 m	17	68	68	68	68	273	273	273	273	273
FLOSS, 15 m	17	34	68	68	273	273	137	273	273	273
FLOSS, 20 m	17	273	68	68	273	273	137	273	273	273
FLOSS, 30 m	17	273	137	137	273	273	273	137	273	273
Cruz Alta, 2.5 m	51	51	102	102	205	205	205	205	205	205
Cruz Alta, 5 m	51	51	102	102	102	205	205	102	205	205
Uatumã	51	102	102	102	102	102	102	205	205	205
Km77	51	51	26	51	51	51	51	51	51	205
São João	51	51	51	102	102	205	102	205	205	205
Manaus	51	102	102	102	102	205	205	205	205	205

processes. To do that, therefore, it is important to choose those ratios at time scales that minimize such contribution. According to the discussion at the previous subsection, the minima of ratios $\sigma_V u_*^{-1}$ and eu_*^{-2} in terms of time scale are the best possible choice, and are used here. However, such simple criterion does not apply for ratios $\sigma_w u_*^{-1}$ and $\sigma_\theta \theta_*^{-1}$, which do not always show a minimum. In these cases, the ratios are taken at time scale t_{sm}, the same method used to determine the value of $z\Lambda^{-1}$ for each class of data, as discussed in section 4 and shown in Fig. 4. For reference, t_{sm} values found at all sites and for all classes of stability are shown in Table 3. Its dependence on intensity of turbulence is clear, as the largest values are always found at the most turbulent classes and as more turbulent sites tend to have larger t_{sm} than the less turbulent ones.

It is clear that even when such a careful procedure aiming at minimizing the influence of submeso processes is taken, there is still large site-to-site variability of the dimensionless ratios dependence on the local stability parameter $z\Lambda^{-1}$ (Fig. 8). Of all ratios considered, $\sigma_w u_*^{-1}$ has least site dependence (Fig. 8, top-left panel), which is expected as this ratio is not as affected by submeso processes as the others are. The neutral limit of this ratio coincides across the different sites, with the notable exception of Manaus (symbol m), but larger variability is noticeable under stronger stability.

On the other hand, the dimensionless ratios that involve variances of the horizontal components, $\sigma_V u_*^{-1}$ and eu_*^{-2} (Fig. 8, top-right and bottom-left panels, respectively) are site dependent even in the neutral limit. Such a limit for $\sigma_V u_*^{-1}$ approaches 2.4 at Uatumã, 2.5 at Cruz Alta, and 3.0 at FLOSS—a 25% increase from the smallest to the largest value, despite the fact that it has been determined from the time scale that is least affected by submeso motions. For eu_*^{-2}, the neutral limits

range from 3.6 in Uatumã to 5.0 in FLOSS—a 39% increase from the smallest to the largest value. These discrepancies are enhanced at larger stabilities so that, as an example, at $z\Lambda^{-1} = 1$, the ratio eu_*^{-2} is, in average 6.1 at Uatumã, 7.3 at Cruz Alta, 9.5 at FLOSS 10-m level, and reaches 14 at the lowest level (1 m) from FLOSS. Such contrasting values among the different sites are not, however, surprising. A review of expressions for eu_*^{-2} from the literature shows even larger variability. Panofsky and Dutton (1984) cite a variety of previous observational studies that found the neutral value of eu_*^{-2} ranging from 5.21 to 6.15 over flat terrain and from 6.23 to 18.10 over rolling terrain. Still under neutral stability, values found in more recent studies include 4.52 (Quan and Hu 2009) and 5.38 (Wood et al. 2010) over urban terrain and 5.25 (Pahlow et al. 2001) over flat terrain and 6.02 over complex terrain (Moraes et al. 2005). Under more stable conditions, $z\Lambda^{-1} = 1$, the fitting expressions proposed in the aforementioned studies lead to eu_*^{-2} values of 7.30 (Wood et al. 2010), 8.57 (Quan and Hu 2009), 17.06 (Moraes et al. 2005), and 29.12 (Pahlow et al. 2001). Despite the appreciable variability observed, in general the different sites from the present studies showed smaller values than those found in the literature, both for neutral and more stable conditions—a consequence of the effort presently taken to minimize the influence of submeso processes.

Two pieces of evidence sustain the hypothesis that most of the site-to-site variability of the dimensionless ratios arise from the distinct influence of submeso processes over the regions being considered. The first is the fact that $\sigma_w u_*^{-1}$ is the ratio that shows the least site dependence, which is consistent with the absence of submeso contribution to σ_w, and also showing that most of the submeso contribution to u_* happens at time scales larger than t_{sm}. The second indication comes from the fact that ratios $\sigma_V u_*^{-1}$ and eu_*^{-2}, dependent on horizontal motion, and, therefore, largely affected by submeso processes tend to be larger at those sites where this sort of phenomena are more important, such as FLOSS or Km77, and smaller where they tend to be less relevant, such as Cruz Alta or Uatumã.

Is it possible to find site-independent expressions for those ratios and their stability dependence? Or, assuming the hypothesis that the variability is caused by submeso contribution is correct, how can one find expressions that are as unaffected by such an influence as possible?

To do that, the observations from all different sites are considered together, and their values are classified by R_{sm}, the submeso relative importance with respect to the turbulent motion, defined at section 4 as $R_{sm} = e_{sm}/\sigma_w$.

The relative independence of $\sigma_w u_*^{-1}$ on the submeso forcing, quantified by R_{sm}, becomes even more evident,
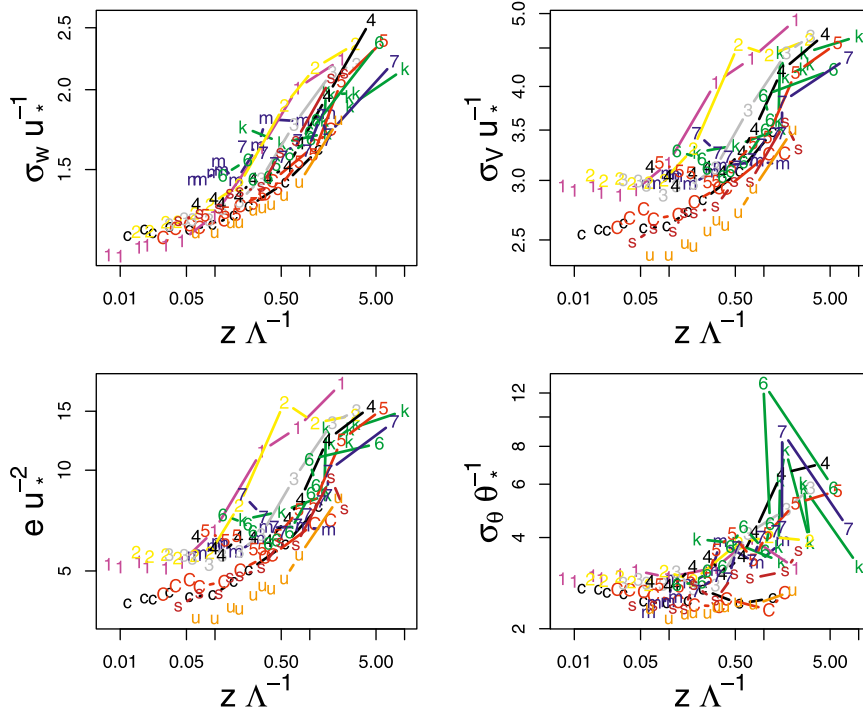
FIG. 8. Comparison of the dependence of ratios (top left) $\sigma_w u_*^{-1}$, (top right) $\sigma_V u_*^{-1}$, (bottom left) eu_*^{-2}, and (bottom right) $\sigma_\theta \theta_*^{-1}$ on the local stability parameter $z\Lambda^{-1}$ among the different sites and levels used. The symbols that represent each site and level are the same as described in Fig. 1. For each site and level, 10 points are plotted, corresponding to the 10 classes of σ_w considered.

as no clear distinction exists among the different classes of R_{sm} (Fig. 9, top-left panel). The expression that best adjusts the data from all experiments considered in the present study is $\sigma_w u_*^{-1} = 1.2(1 + 3.6z\Lambda^{-1})^{0.2}$, which is compared in Fig. 9 to other expressions from the literature. Toward neutrality, this expression approaches that proposed by Pahlow et al. (2001), while in more stable conditions it tends toward the expression proposed by Quan and Hu (2009).

Interestingly, and entirely supporting the hypothesis that most of the site variability observed on the dimensionless ratios is caused by submeso influence, both $\sigma_V u_*^{-1}$ (Fig. 9, top-right panel) and eu_*^{-2} (Fig. 9, bottom-left panel) are highly dependent on R_{sm}. This is evidenced by the fact that different and well-behaved dependencies of these ratios on $z\Lambda^{-1}$ exist for each class of R_{sm} considered. The simplest choice for an expression that minimizes the submeso influence and its associated site dependence is a fitting to the data from the lowest R_{sm} class. However, it can be seen in Fig. 9 that such lowest R_{sm} class spans a limited stability range and that such a range is progressively expanded at classes of larger R_{sm}. Therefore, the proposed expressions for $\sigma_V u_*^{-1}$ and eu_*^{-2} in terms of $z\Lambda^{-1}$ represent fittings to

the lowest envelope of points in Fig. 9 (top-right and bottom-left panels): $\sigma_V u_*^{-1} = 2.6(1 + 0.5z\Lambda^{-1})^{1/3}$ and $eu_*^{-2} = 4(1 + 2.5z\Lambda^{-1})^{1/3}$. For both ratios, the respective expressions fall below those previously proposed, which is a direct consequence of the attempt to minimize the submeso influence on the result. Nevertheless, it is possible that some low-frequency motions are still affecting the result, especially at large stability, as in such case the fitting arises from points with reasonably large R_{sm}. On the other hand, the adjustment in more neutral conditions is proportioned solely by cases with fairly small submeso contribution, making it likely that the purely turbulent value of eu_*^{-2} at neutral conditions approaches 4. It is interesting here to notice that this value is close to the 3.75 used by Wyngaard (1975) in his pioneer efforts on modeling the SBL.

A more complex situation occurs for $\sigma_\theta \theta_*^{-1}$ (Fig. 9, bottom-right panel), as its dependency on $z\Lambda^{-1}$ for the different R_{sm} classes are not clearly distinct from each other. Nevertheless, some distinct patterns can be observed. First, the values of $\sigma_\theta \theta_*^{-1}$ consistently tend to be larger in classes of larger submeso influence. Furthermore, at each class a significant increase of $\sigma_\theta \theta_*^{-1}$ occurs at the limit of small $z\Lambda^{-1}$. The reason for such large
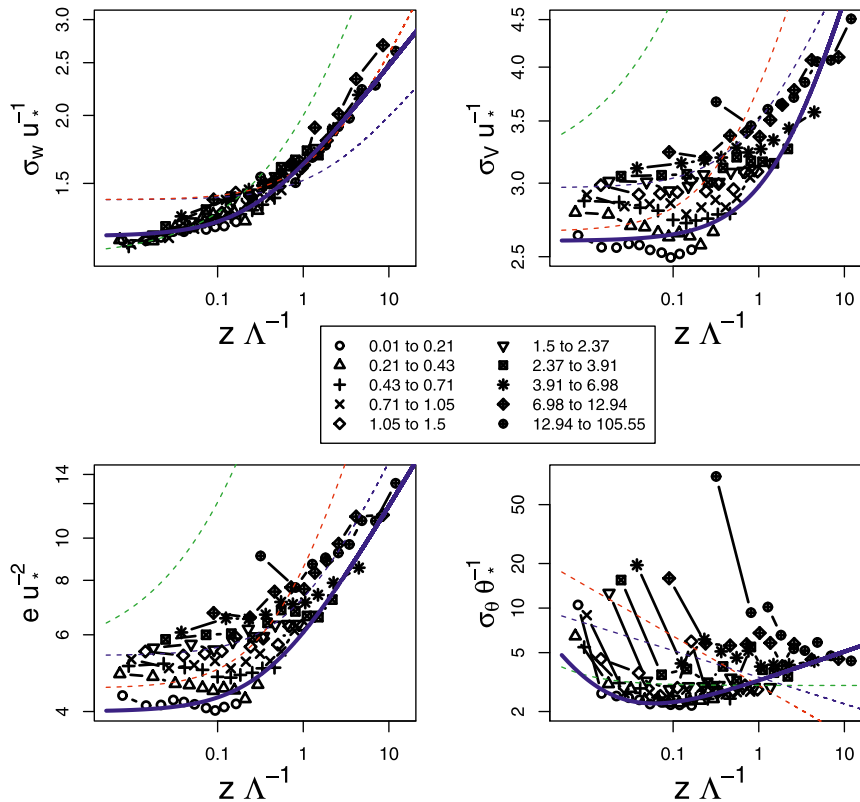
FIG. 9. Dependence of ratios (top left) $\sigma_w u_*^{-1}$, (top right) $\sigma_V u_*^{-1}$, (bottom left) eu_*^{-2}, and (bottom right) $\sigma_\theta \theta_*^{-1}$ on the local stability parameter $z\Lambda^{-1}$ for different classes of R_{sm} as indicated by legend, using the data from all sites and levels together. In all panels, thick blue line is the fitting to the lower envelope of data proposed in the present study, while green dashed lines correspond to the expressions proposed by Pahlow et al. (2001), the red dashed lines were proposed by Quan and Hu (2009), and the blue dashed lines were proposed by Wood et al. (2010).

values at the lowest stability within each class can be understood if one analyses the S_θ spectra shown in Figs. 2a and 2b (bottom-left panels). Both at FLOSS and Cruz Alta (and at the other sites as well), and for all classes of σ_w, the sharp increase of S_θ occurs at smaller time scales than the sharp increase of other variables, such as S_e. As a consequence, it is possible that such an increase in temperature fluctuations occurs at smaller time scales than t_{sm}, chosen as the lower limit for the submeso range. As the ratio $\sigma_\theta \theta_*^{-1}$ is evaluated at t_{sm}, it may be affected by the sharp increase of S_θ, associated with submeso temperature fluctuations. At each class of R_{sm}, such a problem becomes more critical at the lower limit of $z\Lambda^{-1}$ because these are the cases when S_θ increases at smallest time scales. In fact, such an increase of S_θ at smaller time scales than other variables imposes an additional difficulty for finding the correct value of $\sigma_\theta \theta_*^{-1}$ at the neutral limit, because it is possible that this ratio is affected by submeso processes even at time scales where other ratios are not. Dias et al. (1995) reviewed previous

studies, finding that the neutral limit of $\sigma_\theta \theta_*^{-1}$ ranges from 1.7 to 3.0. It is possible that most of such variability is associated to the fact just described. Despite this specific difficulty at lower stability, the values of $\sigma_\theta \theta_*^{-1}$ for different classes of R_{sm} collapse toward larger values of $z\Lambda^{-1}$ and, for this reason, the lower envelope of data is again a good estimate for the stability dependence of $\sigma_\theta \theta_*^{-1}$ that is least influenced by submeso. A good fitting to that lower envelope is given by expression $\sigma_\theta \theta_*^{-1} = 3.2(z\Lambda^{-1})^{-1}(0.012 + z\Lambda^{-1})^{1.2}$ (thick blue line in Fig. 9, bottom-left panel). Such an expression has an important difference from those proposed by previous studies, such as Pahlow et al. (2001), Quan and Hu (2009), or Wood et al. (2010). While in all those cases $\sigma_\theta \theta_*^{-1}$ decreases monotonically with stability, the expression presently suggested has a minimum at intermediate stability, near $z\Lambda^{-1} = 0.06$. On the other hand, the proposed expression agrees very closely with the observations by Mahrt et al. (1998) and by Conangla et al. (2008) who also found a minimum for the ratio, at

similar values of stability as in the present study. Such a minimum is associated with a maximum of the absolute heat flux, which tends to zero at neutral conditions as a consequence of reduced thermal gradients, and also tends to zero at very stable conditions, owing to reduced turbulent mixing (Mahrt et al. 1998). As examples, Mahrt et al. (1998) found the maximum heat flux at $zL^{-1} = 0.06$, Moraes et al. (2004) found it at $zL^{-1} = 0.08$, and Malhi (1995) found it at $zL^{-1} = 0.2$—all values near the minimum of the expression currently proposed for the $\sigma_\theta \theta_*^{-1}$ dependence on stability.

6. Conclusions

Along the present study, a number of strong evidences gathered from the comparison of data collected at six reasonably different sites have been shown to sustain the hypothesis that the site-to-site variability observed in similarity relationships at the stable boundary layer (SBL) are associated with locally dependent nonturbulent processes, recently referred as submeso (Mahrt 2010). No effort has been made here to address the mechanisms that generate submeso flow or whether these processes may contribute to turbulence generation by enhancing the wind shear. These are, obviously, extremely important and complex questions that demand specific studies for those purposes and the present results evidence the necessity for better understanding these issues.

Another important finding of the study was the observation that turbulent kinetic energy increases exponentially with time scale in the submeso range and that the rate of increase is larger for less turbulent situations. This result has important implications for subsequent research. One of them is that it allows determining a submeso time-scale t_{sm} and a measure of the relative importance of submeso processes with respect to turbulence, here defined as R_{sm}. Besides, it provides a direct association between the low-frequency phenomena, which may be observed even in simple weather stations, to the turbulent portion of the flow.

A very important, yet unanswered question regarding the role of nonturbulent processes in the stable boundary layer regards how they can be modeled. The present analysis has shown that it is possible to determine, for each case, the value of the similarity ratios that minimizes the submeso influence, although without entirely removing it. Applying this methodology, novel expressions for the dependences of dimensionless ratios on the stability parameter have been proposed, and these are expected to be a better representation of purely turbulent flow in the SBL than those obtained previously without similar concern with the role of nonturbulent processes. For this reason, these expressions are well suited to the application in models of purely turbulent exchange in the nocturnal boundary layer. However, previous studies have shown that the inclusion of submeso processes improves the closure of scalar budgets (Acevedo and Mahrt 2010; Kidston et al. 2010). It means that for applied purposes, such as weather or air quality forecasting, the submeso processes that have been carefully removed in the present study frequently have an important role. Ideally, then, a model study with those goals should use locally found similarity expressions that include both the universal turbulent and the local submeso components. However, this is often not feasible and may not even be useful because of the highly variable nature of the submeso processes. Furthermore, local expressions would be necessary for each place and condition being simulated. For all these reasons, it is clear that a better physical understanding of the processes that cause the submeso flow is necessary, so that they can be incorporated to models in terms of the external features that control them. This knowledge does not yet exist and its necessity is evident. Once this is achieved, locally dependent formulations of nonturbulent processes may be added, in models, to the universal functions that represent the turbulent portion of the flow, such as those provided by the present study.

REFERENCES

Acevedo, O. C., and L. Mahrt, 2010: Systematic vertical variation of mesoscale fluxes in the nocturnal boundary layer. *Bound.-Layer Meteor.,* **135,** 19–30.

——, O. L. L. Moraes, D. R. Fitzjarrald, R. K. Sakai, and L. Mahrt, 2007: Turbulent carbon exchange in very stable conditions. *Bound.-Layer Meteor.,* **125,** 49–61.

——, ——, G. A. Degrazia, D. R. Fitzjarrald, A. O. Manzi, and J. G. Campos, 2009: Is friction velocity the most appropriate scale for correcting nocturnal carbon dioxide fluxes? *Agric. For. Meteor.,* **149,** 1–10.

Andrén, A., 1990: Evaluation of a turbulence closure scheme suitable for air-pollution applications. *J. Appl. Meteor.,* **29,** 224–239.

Araujo, A. C., and Coauthors, 2002: Comparative measurements of carbon dioxide fluxes from two nearby towers in a central Amazonian rain forest: The Manaus LBA site. *J. Geophys. Res.,* **107,** 8090, doi:10.1029/2001JD000676.

Baas, P., G. J. Steeneveld, B. J. H. van de Wiel, and A. A. M. Holtslag, 2006: Exploring self-correlation in flux–gradient relationships for stably stratified conditions. *J. Atmos. Sci.,* **63,** 3045–3054.

——, S. R. de Roode, and G. Lenderink, 2008: The scaling behaviour of a turbulent kinetic energy closure model for stably stratified conditions. *Bound.-Layer Meteor.,* **127,** 17–36.

Belušić, D., and I. Güttler, 2010: Can mesoscale models reproduce meandering motions? *Quart. J. Roy. Meteor. Soc.,* **136,** 553–565.

Burns, S., and Coauthors, 2010: Atmospheric stability effects on wind fields and scalar mixing within and just above a subalpine forest in sloping terrain. *Bound.-Layer Meteor.,* **138,** 231–262.

Conangla, L., J. Cuxart, and M. R. Soler, 2008: Characterisation of the nocturnal boundary layer at a site in northern Spain. *Bound.-Layer Meteor.,* **128,** 255–276.

Costa, F. D., O. C. Acevedo, J. C. M. Mombach, and G. A. Degrazia, 2011: A simplified model for intermittent turbulence in the nocturnal boundary layer. *J. Atmos. Sci.,* **68,** 1714–1729.

Cuxart, J., and Coauthors, 2006: Single-column model intercomparison for a stably stratified atmospheric boundary layer. *Bound.-Layer Meteor.,* **118,** 273–303.

Dias, N. L., W. Brutsaert, and M. L. Wesely, 1995: Z-less stratification under stable conditions. *Bound.-Layer Meteor.,* **75,** 175–187.

Duynkerke, P., 1988: Application of the $E - \varepsilon$ turbulence closure model to the neutral and stable atmospheric boundary layer. *J. Atmos. Sci.,* **45,** 865–880.

Finnigan, J. J., 2010: Waving plants and turbulent eddies. *J. Fluid Mech.,* **652,** 1–4.

——, R. H. Shaw, and E. G. Patton, 2009: Turbulence structure above a vegetation canopy. *J. Fluid Mech.,* **637,** 387–424.

Howell, J. F., and L. Mahrt, 1997: Multiresolution flux decomposition. *Bound.-Layer Meteor.,* **83,** 117–137.

Kidston, J., C. Brummer, T. A. Black, K. Morgenstern, Z. Nesic, J. H. McCaughey, and A. G. Barr, 2010: Energy balance closure using eddy covariance above two different land surfaces and implications for CO_2 flux measurements. *Bound.-Layer Meteor.,* **136,** 193–218.

Klipp, C. L., and L. Mahrt, 2004: Flux-gradient relationship, self-correlation and intermittency in the stable boundary layer. *Quart. J. Roy. Meteor. Soc.,* **130,** 2087–2103.

Mahrt, L., 2009: Characteristics of submeso winds in the stable boundary layer. *Bound.-Layer Meteor.,* **130,** 1–14.

——, 2010: Variability and maintenance of turbulence in the very stable boundary layer. *Bound.-Layer Meteor.,* **135,** 1–18.

——, 2011: The near-calm stable boundary layer. *Bound.-Layer Meteor.,* **140,** 343–360.

——, and D. Vickers, 2005: Boundary-layer adjustment over small-scale changes of surface heat flux. *Bound.-Layer Meteor.,* **116,** 313–330.

——, and R. Mills, 2009: Horizontal diffusion by submeso motions in the stable boundary layer. *Environ. Fluid Mech.,* **9,** 443–456.

——, J. Sun, W. Blumen, T. Delany, and S. Oncley, 1998: Nocturnal boundary-layer regimes. *Bound.-Layer Meteor.,* **88,** 255–278.

——, C. Thomas, S. Richardson, N. Seaman, D. Stauffer, and M. Zeeman, 2013: Non-stationarity generation of weak turbulence for very stable and weak-wind conditions. *Bound.-Layer Meteor.,* **147,** 179–199, doi:10.1007/s10546-012-9782-x.

Malhi, Y. S., 1995: The significance of the dual solutions for heat fluxes measured by the temperature fluctuation method in stable conditions. *Bound.-Layer Meteor.,* **74,** 389–396.

Mallat, S., 1989: A theory for multiresolution signal decomposition: The wavelet representation. *IEEE Trans. Pattern Anal. Mach. Intell.,* **11,** 674–693.

Mauritsen, T., and G. Svensson, 2007: Observations of stably stratified shear-driven atmospheric turbulence at low and high Richardson numbers. *J. Atmos. Sci.,* **64,** 645–655.

Monti, P., H. J. S. Fernando, M. Princevac, W. C. Chan, T. A. Kowalewski, and E. R. Pardyjak, 2002: Observations of flow and turbulence in the nocturnal boundary layer over a slope. *J. Atmos. Sci.,* **59,** 2513–2534.

Moraes, O. L. L., O. C. Acevedo, R. Silva, R. Magnago, and A. C. Siqueira, 2004: Nocturnal surface-layer characteristics at the bottom of a valley. *Bound.-Layer Meteor.,* **112,** 159–177.

——, ——, G. A. Degrazia, D. Anfossi, R. Silva, and V. Anabor, 2005: Surface layer turbulence parameters over a complex terrain. *Atmos. Environ.,* **39,** 3103–3112.

Oliveira, P. E. S., O. C. Acevedo, O. L. L. Moraes, H. R. Zimmermann, and C. Teichrieb, 2013: Nocturnal intermittent coupling between the interior of a pine forest and the air above it. *Bound.-Layer Meteor.,* **146,** 45–64.

Pahlow, M., M. B. Parlange, and F. Porté-Agel, 2001: On Monin–Obukhov similarity in the stable atmospheric boundary layer. *Bound.-Layer Meteor.,* **99,** 225–248.

Panofsky, H. A., 1973: Tower micrometeorology. *Workshop on Micrometeorology,* D. A. Haugen, Ed., Amer. Meteor. Soc., 151–176.

——, and J. A. Dutton, 1984: *Atmospheric Turbulence.* Wiley and Sons, 397 pp.

Quan, L., and F. Hu, 2009: Relationship between turbulent flux and variance in the urban canopy. *Meteor. Atmos. Phys.,* **104,** 29–36.

Sakai, R. K., and Coauthors, 2004: Land-use effects on local energy, water and carbon balances in an Amazonian agricultural field. *Global Change Biol.,* **10,** 895–907.

Sun, J., L. Mahrt, R. M. Banta, and Y. L. Pichugina, 2012: Turbulence regimes and turbulence intermittency in the stable boundary layer during CASES-99. *J. Atmos. Sci.,* **69,** 338–351.

Teichrieb, C. A., O. C. Acevedo, G. A. Degrazia, O. L. L. Moraes, D. R. Roberti, H. R. Zimmermann, D. M. Santos, and R. C. M. Alves, 2013: Characterizing the relative role of low-frequency and turbulent processes in the nocturnal boundary layer through the analysis of two-point correlations of the wind components. *Physica A,* **392,** 1510–1521.

Thomas, C. K., 2011: Variability of sub-canopy flow, temperature and horizontal advection in moderately complex terrain. *Bound.-Layer Meteor.,* **139,** 61–81.

——, J. G. Martin, B. E. Law, and K. Davis, 2013: Toward biologically meaningful net carbon exchange estimates for tall, dense canopies: Multi-level eddy covariance observations and canopy coupling regimes in a mature Douglas-fir forest in Oregon. *Agric. For. Meteor.,* **173,** 14–27.

Vickers, D., and L. Mahrt, 2003: The cospectral gap and turbulent flux calculations. *J. Atmos. Oceanic Technol.,* **20,** 660–672.

——, and ——, 2007: Observations of the cross-wind velocity variance in the stable boundary layer. *Environ. Fluid Mech.,* **7,** 55–71.

Vindel, J. M., and C. Yagüe, 2011: Intermittency of turbulence in the atmospheric boundary layer: Scaling exponents and stratification influence. *Bound.-Layer Meteor.,* **140,** 73–85.

Wood, C. R., and Coauthors, 2010: Turbulent flow at 190 m height above London during 2006-2008: A climatology and the applicability of similarity theory. *Bound.-Layer Meteor.,* **137,** 77–96.

Wyngaard, J. C., 1975: Modeling the planetary boundary layer—Extension to the stable case. *Bound.-Layer Meteor.,* **9,** 441–460.